Bone 120 (2019) 25–37

Contents lists available at ScienceDirect

Bone

journal homepage: www.elsevier.com/locate/bone

Full Length Article

Biofidelic finite element models for accurately classifying hip fracture in a retrospective clinical study of elderly women from the AGES Reykjavik cohort

W.S. Enns-Bray[a], H. Bahaloo[b], I. Fleps[a], Y. Pauchard[c], E. Taghizadeh[d], S. Sigurdsson[e], T. Aspelund[e], P. Büchler[d], T. Harris[f], V. Gudnason[e], S.J. Ferguson[a], H. Pálsson[b], B. Helgason[a,g,*]

[a] Institute for Biomechanics, ETH Zürich, Zürich, Switzerland
[b] School of Engineering and Natural Sciences, University of Iceland, Reykjavik, Iceland
[c] McCaig Institute for Bone and Joint Health, University of Calgary, Calgary, Canada
[d] Institute for Surgical Technology and Biomechanics, University of Bern, Bern, Switzerland
[e] The Icelandic Heart Association Research Institute, Kopavogur, Iceland
[f] Laboratory of Epidemiology and Population Sciences, National Institute on Aging, Bethesda, MD, USA
[g] School of Science and Engineering, Reykjavik University, Reykjavik, Iceland

ARTICLE INFO

Keywords:
Hip fracture
Clinical retrospective
Finite element
Sideways fall
Computed tomography

ABSTRACT

Clinical retrospective studies have only reported limited improvements in hip fracture classification accuracy using finite element (FE) models compared to conventional areal bone mineral density (aBMD) measurements. A possible explanation is that state-of-the-art quasi-static models do not estimate patient-specific loads. A novel FE modeling technique was developed to improve the biofidelity of simulated impact loading from sideways falling. This included surrogate models of the pelvis, lower extremities, and soft tissue that were morphed based on subject anthropometrics. Hip fracture prediction models based on aBMD and FE measurements were compared in a retrospective study of 254 elderly female subjects from the AGES-Reykjavik study. Subject fragility ratio (FR) was defined as the ratio between the ultimate forces of paired biofidelic models, one with linear elastic and the other with non-linear stress-strain relationships in the proximal femur. The expected end-point value (EEV) was defined as the FR weighted by the probability of one sideways fall over five years, based on self-reported fall frequency at baseline. The change in maximum volumetric strain (ΔMVS) on the surface of the femoral neck was calculated between time of ultimate femur force and 90% post-ultimate force in order to assess the extent of tensile tissue damage present in non-linear models. After age-adjusted logistic regression, the area under the receiver-operator curve (AUC) was highest for ΔMVS (0.72), followed by FR (0.71), aBMD (0.70), and EEV (0.67), however the differences between FEA and aBMD based prediction models were not deemed statistically significant. When subjects with no history of falling were excluded from the analysis, thus artificially assuming that falls were known a priori with no uncertainty, a statistically significant difference in AUC was detected between ΔMVS (0.85), and aBMD (0.74). Multivariable linear regression suggested that the variance in maximum elastic femur force was best explained by femoral head radius, pelvis width, and soft tissue thickness ($R^2 = 0.79$; RMSE = 0.46 kN; $p < 0.005$). Weighting the hip fracture prediction models based on self-reported fall frequency did not improve the models' sensitivity, however excluding non-fallers lead to significant differences between aBMD and FE based models. These findings suggest that an accurate assessment of fall probability is necessary for accurately identifying individuals predisposed to hip fracture.

1. Introduction

Over 90% of hip fractures are the result of low trauma falls, i.e. falling from standing height or less [1,2]. These injuries can lead to individuals transitioning from community dwelling to institutional care [3], and are associated with residual walking disability [4] and high mortality [5]. An epidemiological study estimated that hip fracture incidence in European countries will rise from 610 thousand fractures in 2010, to 810 thousand by 2025. Meanwhile, the direct medical costs related to hip fracture are expected to reach 25.3 billion euros [6].

* Corresponding author at: Institute for Biomechanics, ETH Zürich, Zürich, Switzerland.
E-mail address: bhelgason@ethz.ch (B. Helgason).

https://doi.org/10.1016/j.bone.2018.09.014
Received 21 March 2018; Received in revised form 10 September 2018; Accepted 17 September 2018
Available online 19 September 2018

Table 1
Subject descriptive statistics with summary of biofidelic simulation results.

	Fracture (N = 95)				Non-fracture (N = 159)				Sub-cohort women (N = 464)				Sub-cohort men (N = 691)			
	Mean	St. Dev.	Max	Min	Mean	St. Dev.	Max	Min	Mean	St. Dev.	Max	Min	Mean	St. Dev.	Max	Min
Age	78.8	5.4	91	67	76.4	5.5	89	67	77.2	5.5	93	66	77.2	5.7	96	67
Height [cm]	159.2	5.88	173.5	145.1	161.17	5.93	175.8	144.4	160.8	5.68	175.9	144.4	175.1	6.2	194.4	159.15
Weight [kg]	65.9	13.0	111.2	36.5	70.8	13.7	133.4	39.9	69.1	13.3	123.3	36.5	81.9	14.2	135.0	49.9
aBMD [g/cm^2]	0.62	0.12	0.96	0.42	0.72	0.15	1.10	0.37	0.68	0.14	1.19	0.32	0.84	0.18	1.49	0.33
FR	1.45	0.32	2.41	1.01	1.24	0.24	2.10	0.99	–	–	–	–	–	–	–	–
ΔMVS	0.11	0.06	0.26	−0.001	0.06	0.07	0.32	−0.02	–	–	–	–	–	–	–	–

Limitations in current standard of care include low diagnostic sensitivity and over diagnosis [7], both of which have likely contributed to the declining number of patients receiving treatment for hip fragility [6]. Thus, the search continues for a new diagnostic technique capable of identifying individuals predisposed to hip fracture.

The conventional diagnosis of hip fragility relies on the definition of osteoporosis as an areal bone mineral density (aBMD) measurement corresponding to 2.5 standard deviations below the mean for a healthy 25-year-old individual of matched gender and ethnicity. However, it is generally accepted that aBMD measured by dual x-ray absorptiometry (DXA) is limited in its ability to predict fracture cases based on the low sensitivity of the osteoporosis threshold (i.e. T-score < 2.5) to fracture incidence reported in prospective studies [8–10]. Alternative diagnostic criteria have been proposed based on finite element analysis (FEA) of the proximal femur derived from quantitative computed tomography (QCT). This technique has proven adept at predicting the mechanical strength of the proximal femur compared to ex vivo experiments [11–13]. However, retrospective studies utilizing this technology have only shown moderate improvements in fracture prediction sensitivity compared to aBMD [14–16].

The performance gap between ex vivo and retrospective studies could be connected to the difference in boundary conditions. State-of-the-art FEA techniques use quasi-static loading to determine the structural load bearing strength of the proximal femur. While this technique is adequate for measuring subject-specific femoral strength, real hip fractures are the result of the femur sustaining an impact load greater than its load bearing capacity. Epidemiological studies have estimated that only 1–5% of falls actually result in fracture [17–19], suggesting that information about fall risk and severity (i.e. the frequency and magnitude of impact loads to the femur) must be combined with estimates of femoral strength in order to accurately assess patient-specific fracture risk.

Previous biomechanical studies have modeled dynamic impact loading of the proximal femur using explicit FE solvers [20–23]. These models utilized non-linear, strain rate dependent properties, and were capable of accurately predicting the impulse response [20] and fracture location [21] when compared to ex vivo, drop tower experiments [24]. Recently, ex vivo experiments using a novel hip impactor apparatus, that included cadaveric femur, pelvis, ligaments, and a soft tissue surrogate, were used to validate biofidelic FE simulations that also included representations of these additional boney structures and connective tissues [25].

The present study aimed to compare hip fracture classification models based on measurements from biofidelic hip impact simulations to aBMD measurements in a large retrospective study of clinical data. We hypothesized that incorporating additional subject-specific information regarding the pelvis, lower extremities, and soft tissue would improve the sensitivity and specificity of the resulting hip fracture classification model compared to previous retrospective studies. An alternative hypothesis was also tested for a subset of subjects that either reported a history of falling, or suffered hip fracture during the monitoring period. This was designed to exclude subjects that never fell, thereby eliminating the effect of fall risk uncertainty, which could confound the different hip fracture predictors. Additionally, this study aimed to quantify the subject-specific impact force sustained by the femur as function of subject anthropometrics, including height, weight, bone geometry, and soft tissue thickness.

2. Materials and methods

2.1. Subject selection

The AGES-Reykjavik cohort includes 4800 baseline CT scans of the hips of elderly men and women. Subjects were monitored between four to seven years after enrollment, during which any hip fractures were registered within the database [26]. Using a case-cohort study design, 377 subjects were first selected based on medical records of hip fracture in accordance with ICD-10 codes. Next, a control subcohort of 778 subjects was randomly selected to establish an overall case-control ratio of approximately 1:2. The whole subcohort included 1155 men and women, and the present study reports the preliminary results of the first 254 women randomly selected from this subcohort. One subject was excluded due to the CT scan being unsuitable for FEA. Descriptive statistics for the 254 subjects tested in the present study are detailed in Table 1. Since DXA scans were not available, total femur aBMD was calculated in g/cm^2 from baseline CT scans that were calibrated to g/cm^3 of calcium hydroxyapatite, in a DXA-equivalent region used to clinically assess osteoporosis. This approach was similar to previous finite element studies using the AGES-RS cohort [14,15], as high correlations have been reported between DXA-based and QCT-based aBMD measurements [27].

2.2. CT scans

All CT scans were obtained from the same scanner (Siemens Sensation 4) using 120 kVp, a pitch of 1.0, and a modulated tube current with a reference exposure of 150 mAs. Images were reconstructed using a 1.0 mm slice thickness, with $1 \times 1 \times 1$ mm voxel size, a B30s soft-tissue kernel, and a 50-cm field of view. A bone mineral density calibration phantom (Image Analysis, Columbia, KY, USA) was present in every scan, located under the spine and extending from the lower femoral shaft up to the vertebral body. The three phantom calibration cells had a concentration of 0, 75 and 150 mg/cm^3 of calcium hydroxyapatite, respectively, which was extracted from each CT stack and used for calibration [28].

2.3. Finite element analysis

2.3.1. Femur on impact side

An overview of the pipeline used to generate subject-specific biofidelic models is presented in Fig. 1. Surface geometry of the left proximal femur was segmented using the semi-automated graph-cut method within the open-source software platform MITK-GEM [29]. Proximal femur volumes were meshed with 10-node tetrahedral elements with a target length of 3 mm using ANSA (v17.0, BETA CAE Systems, Thessaloniki, Greece).

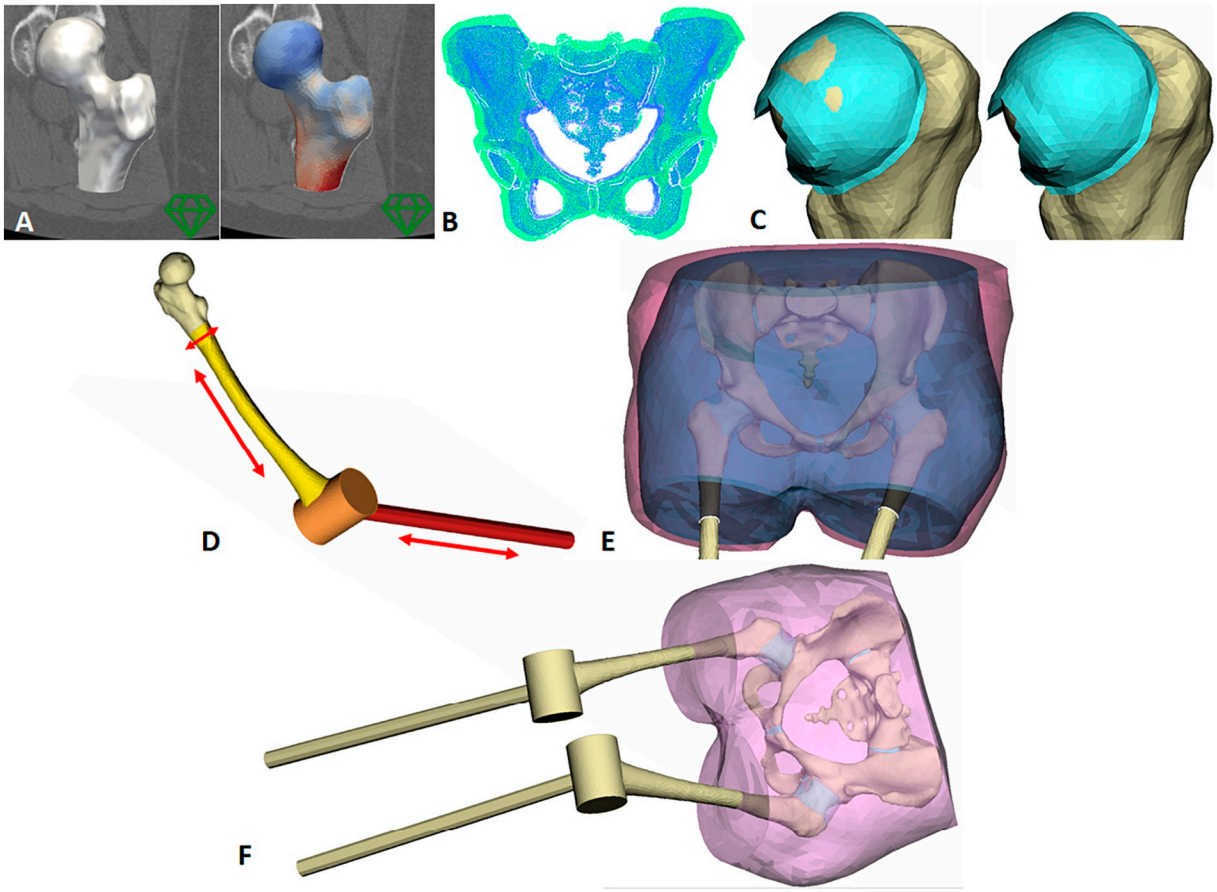

Fig. 1. Overview of biofidelic hip modeling pipeline, including A: femur segmentation and material mapping. B: Pelvis morphing based on subject-specific pelvis width and femoral head radius. C: Articular cartilage was morphed to the surface of the femoral head. D: The lower extremities were morphed based on subject height and femur diameter. E: The soft tissue shape was selected based on subject hip circumference and morphed according to the calculated subject-specific fall inertia. F: The finished model in fall alignment.

2.3.2. *Pelvis and contralateral femur*

The template models of the pelvis and right femur were derived from a CT scan of a 62-year-old female (femoral neck T-score: −0.91) used in a previous experimental validation study [25]. The bone geometry was segmented, meshed, and mapped using the same methodology as the left femur, albeit using 4-node tetrahedral elements. The pelvis and right femur models were assigned strain-rate dependent material properties with linear elastic stress-strain relationships. Material properties for the cartilage and ligaments were based on previously published experiments using location-specific human tissue, and are described in Table 2. Acetabular cartilage was modeled using a non-viscous, general hyper-elastic rubber model based on mechanical tests of human acetabular cartilage [30]. Nodes of elements representing acetabular cartilage were either tied to pelvis elements or morphed to the surface of the femoral head. Pelvis cartilage was also modeled within the pubic symphysis and sacroiliac joints using a Mooney-Rivlin hyper-elastic model based on drop tower testing of lateral impacts to the pubic cartilage of isolated human pelvic bones [31]. Pelvis ligaments were modeled using tension only cable elements with fully elastic properties based on experiments applying vertical loads to human pelvis ligaments [32].

The surrogate pelvis model was morphed according to subject-

Table 2
Material properties and material models for cartilage, ligaments, and soft tissue components.

Model component	LD-DYNA material model	Material parameters	Tissue tested	Reference
Acetabular cartilage	MAT77 (MAT_HYPERELASTIC RUBBER)	Rho = 1.0 g/cm^2, C10 = 0.3516 MPa, C01 = 0.3059 MPa, C11 = 0.05235 MPa, μ = 0.495	Femoral head cartilage	[30]
Sacroilliac & pubis cartilage	MAT27 (MAT_MOONEY-RIVLIN_RUBBER)	Rho = 1.0 g/cm^2, C10 = 0.1 MPa, C01 = 0.45 MPa, μ = 0.495	Reverse engineered from whole pubic symphysis	[31]
Pelvis ligaments	MAT71 (MAT_CABLE_DISCRETE_BEAM) (tension only)	Rho = 1.0 g/cm^2, E = 395 MPa	Iliotibial tract stiffness	[32]
Capsular ligaments	MAT1 (MAT_elastic)	Rho = 1.05 g/cm^2, E = 2 MPa, μ = 0.3, Ipsilateral side models toe region of ligament stress-strain curve (contralateral side: E = 200, contralateral side models ligament tensile stiffness beyond toe region)	Capsular ligament in tension	–
Soft tissue	MAT31 (MAT_FRAZER_NASH_RUBBER)	Rho = 1.05 g/cm^2, C100 = 1.08 × 10^{-2} MPa, C200 = 2.242 × 10^{-4} MPa, C11 = 2.1709 × 10^{-6} MPa	20% Ballistic gelatin in tension, compression and indentation	[25]

specific anatomical geometry in two steps using in-house Python scripts, based on morphing functions within ANSA. First, the articulating surface of the impacted acetabular cup was scaled spherically, centered at the native femoral head center, according to the ratio between native and subject-specific femur head radii. Elements within sections of the adjacent the ilium, ischium, and pubis bones were morphed to accommodate the scaling of the acetabulum by maintaining their smooth anatomical shape. The purpose of this adjustment was to ensure a realistic joint contact between the pelvis and the subject-specific femur model during impact. Subsequently, the entire pelvic inlet was radially scaled, centered at the center of gravity of the elements defining the pelvic inlet, such that surrogate pelvis had that same pelvic width as the subject, which was defined as the distance between the femoral head centers, minus the radii of the femoral heads. To accommodate the scaling of the pelvic inlet, the remaining surfaces of the ilium, ischium, and pubis bones not included in the inlet were morphed in order to maintain an anatomically realistic pelvis, and eliminate any artifacts or sharp edges resulting from scaling. Adjusting the pelvis geometry in this manner was essential in order to match the subject's pelvis width, which later determined the soft tissue thickness covering the impacted femur. The surrogate right (non-impacted) femur model was not morphed. All morphing procedures developed in this study were fully automated after defining the relevant anatomical regions being morphed, allowing an identical implementation for every subject.

Capsular ligaments connecting the femurs to the pelvis were modeled with linear 5 mm shell elements, 1 mm thick, with an elastic modulus of 2 MPa. Preliminary testing indicated that femur impact force was not sensitive to the tensile properties of the capsular ligaments, therefore the purpose of modeling the capsular ligament was only to prevent solid soft tissue elements from being generated within the joint capsule.

2.3.3. Material mapping strategy for bone tissue

The tissue modulus of elasticity (E) of each element representing bone tissue was calculated according to METHOD B from a previous study comparing different material mapping strategies [33], which included partial-volume artifact correction on the cortical surface. Briefly, CT units within the scans were converted to mg Hydroxyapatite (mgHA) using linear interpolation based on the bone mineral phantom included in every scan. Ash density (ρ_{ash}) was calculated according to $\rho_{ash} = (mgHA/1000 + 0.09) / 1.14$ [g/cm^3], and subsequently converted to apparent density (ρ_{app}) according to $\rho_{app} = \rho_{ash} / 0.6$ [g/cm^3] [34]. The apparent density of each voxel was used to calculate nodal modulus values according to $E = 6850 * \rho_{app}^{1.49}$ [MPa] [35]. Element modulus was then calculated using tri-linear interpolation of the nodal modulus values [36]. Bone elements were assigned isotropic, nonlinear, strain-rate dependent material properties with tension/compression asymmetry, compressive redensification, and tensile damage, based on previous studies where explicit FE models effectively predicted dynamic loading patterns and damage initiation sites compared to drop-tower experiments with cadaver femurs [20,21]. Additionally, a second identical femur model was generated for each subject and assigned strain-rate dependent properties with linear elastic stress-strain relationships in order to measure the ultimate impact force sustained by the femur in the absence of yielding.

2.3.4. Lower extremities

Surrogate shapes of the distal femur and tibia were modeled using linear elastic shell elements with a target length of 5 mm, a constant thickness of 6 mm, and a modulus of 22 GPa. This modulus was based on the maximum cut-off for cortical bone tissue used by the material mapping strategy for both the femurs and the pelvis, and corresponds to an apparent bone density of 2.2 g/cm^3. This ensured that the lower extremities remained relatively rigid, but with similar modulus as the cortical bone at the distal cut-off of the proximal femur model, where the limbs were joined. The length of the thigh and shank bodies was morphed to 24.0% and 25.1% of subject height, respectively [37]. The diameter of the femoral shaft was aligned to the circumference of the distal cutoff of the subject-specific proximal femur model. Mass elements were rigidly fixed to segments along the length of the thigh and shank to simulate the inertia of the soft tissue of the leg, such that the lower thigh and shank accounted for 6.0% and 4.6% of body mass, respectively [37].

2.3.5. Soft tissue

Eight template shapes of the soft tissue volume enveloping the hip were derived from the SizeUSA database (TC^2 Labs Inc. Apex, NC, USA), which comprised 840 body surface scans of women over 55 years of age. The variance of hip circumference (HC) and hip width (HW) within the SizeUSA database, as well as the distributions within the eight

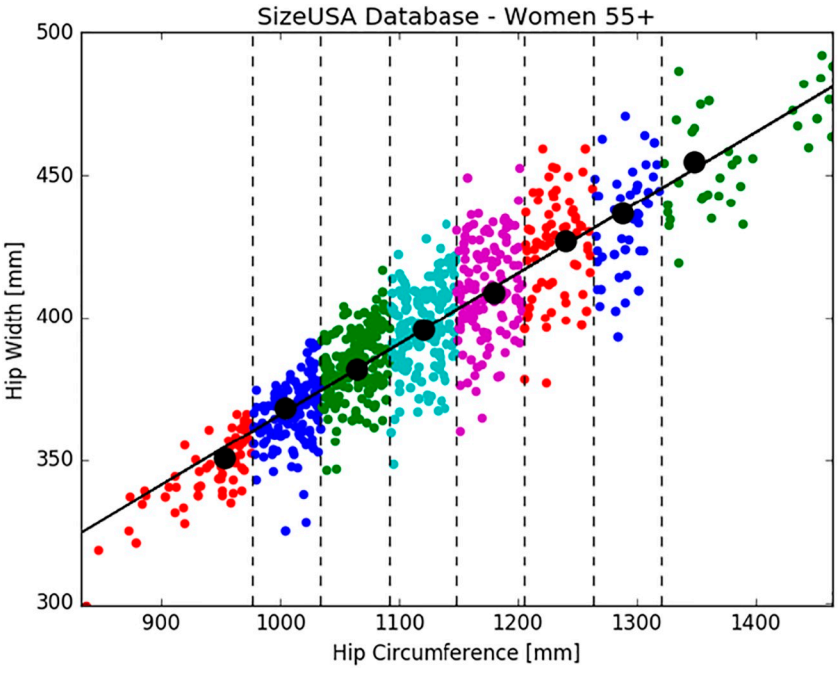

Fig. 2. The hip circumferences and hip widths measured from 840 women over 55 years old in the SizeUSA database, with the eight template bins and a regression line indicating the ideal template shape within each bin. The hip circumference and hip width of the subject selected to represent the bin as the template model is highlighted with a black dot.

different bins represented by the templates, are displayed in Fig. 2. The SizeUSA subject selected as the template surface model for each bin was selected based on the following criteria:

$$Obj = ((HC - HC_{target,i})/HC_{target,i})^2 + ((HW - HW_{target,i})/HW_{target,i})^2$$

$$HC_{target,i} = \mu_{HC} + 0.5 \cdot i \cdot \sigma_{HC}$$

$$HW_{target,i} = A \cdot HC_{target,i} + B$$

$$i = -3, -2, -1, 0, 1, 2, 3, 4$$

where, HC and HW are the hip circumference and hip width of individual subjects from the SizeUSA database, respectively. $HC_{target,\ i}$ and $HW_{target,\ i}$ are the ideal hip circumference and hip width of the eight soft tissue templates, respectively. μ_{HC} and σ_{HC} are the mean and standard deviation of the hip circumference of all subjects in the SizeUSA database, respectively, and A and B are the coefficients of linear regression for HW as a function of HC. HC measurements were defined differently in the SizeUSA database and AGES-Reykjavik cohort, therefore the HC of each AGES subject had to be estimated based on subject BMI using a linear regression model predicting HC as a function of BMI, derived from the SizeUSA database. One of the eight soft tissue template surfaces was subsequently assigned to each AGES subjects based on the nearest matching HC measurements.

The soft tissue modeling methodology was based on the experimental study by Fleps et al. [25], where the soft tissue material properties were based on a ballistic gel designed to represent compressive properties of fat and muscle. Briefly, the selected soft tissue volume was intersected with the lower extremities and a solid mesh was generated with a target element length of 10 mm on the surface, with a gradient to 3 mm on the surface of the femur, pelvis, and lower extremities. Soft tissue nodes were tied to the surface of the other model components. The material properties of the soft tissue (Table 2) were simulated with Frazor-Nash rubber with a Poisson's ratio of 0.495, and other material constants derived from mechanical testing of ballistic gel with properties comparable to human fat and muscle tissue [25].

2.3.6. Boundary conditions and fall inertia

A summary of the landmarking methodology, coordinate systems, and fall alignment is provided in Appendix A. Since only the proximal femur was visible in the CT scans, the distal femur geometry, including the femoral shaft and condyles, had to be estimated using a statistical shape model [38] for the purpose of alignment, using 10 automatically measured landmarks on the femoral head, neck, and greater and lesser trochanters [39]. Anatomical landmarks from the native femur, morphed pelvis template, and statistical shape model of the distal femur, were used to define both femur and pelvis coordinate systems. These coordinate systems provided the basis for transforming the femur, pelvis, and lower extremities into a posterior-lateral fall alignment, designed to represent the most severe hip impact scenario [16,40].

The rigid floor was modeled with a $0.5m^2$ surface of rigid shells, aligned normal to the gravitational vector, and offset 1 mm from the lateral soft tissue surface while centered on the femoral head. A translationally constrained pivot point representing the foot was rigidly fixed to the distal end of the left shank, of the impacted leg, at a point in plane with the floor. A rotational velocity was assigned to the entire model centered at this pivot point, such that the tangential velocity at the point of impact was equal to 3 m/s [41–43].

The soft tissue volume was iteratively morphed such that the rotational inertia of the entire model was equivalent to a theoretical model of the effective mass of the human body during a sideways fall, represented in a linear impact model with one degree of freedom. This approach for calculating subject-specific impact inertia was similar to the experimental validation study using human cadaveric femur and pelvis bones [25]. The soft tissue morphs were automated using in-house python script within ANSA, similar to the pelvis morphs. Four areas in the soft tissue volume were targeted for morphing: the left and right thigh diameters, the anterior abdomen, and the glutes. For the thighs, a ring of elements at the distal cut-off of the soft tissue volume was radially scaled, while the remainder of the thigh volume was automatically morphed to accommodate this scaling. For the anterior abdomen, an approximately 10 cm long row of the most anteriorly protruding surface elements was anteriorly/posteriorly translated, while the entire anterior surface of the abdomen was automatically morphed to accommodate the translation. For the glutes, a ring of elements at the superior cut-off of the soft tissue volume was radially scaled, while morphing the posterior surface of the glutes, plus a waistband of elements within 10 cm of the scaled elements. It is important to note that the lateral surface of the soft tissue covering the impacted femur fixed was left unaffected during morphing in order to preserve the subject-specific soft tissue thickness. These simultaneous morphing procedures effectively to increased or decreased the volume of the soft tissue in an anatomically realistic fashion until the following criteria was met:

$$| I_{zz} - (m_{eff} * R_L^2) | < 0.01 * (m_{eff} * R_L^2)$$

where, m_{eff} is the effective body mass in a sideways fall, which was estimated to be 38% of the total body mass [44,45]. R_L is the length of the axis between the foot point and the lateral surface of the greater trochanter. I_{zz} is the moment of inertia of the entire model around the axis of fall rotation, which was defined as a vector with an origin at the foot point; oriented normal to the plane defined two vectors: the vector between the femoral head and foot point, and the gravitational vector.

2.4. Post processing

2.4.1. Fracture classification and statistical analysis

The impact force applied to the left femur was measured at the contact between the femoral head and acetabulum. The ultimate femur force in the model with linear elastic stress-strain relationships in the femur represented the subject-specific femur load estimated by the simulation. Meanwhile, the ultimate impact force in the model with non-linear femur properties represented the subject-specific ultimate force that the subject's femur was capable of sustaining. The ratio between the ultimate forces measured in the paired linear elastic and non-linear models was termed the fragility ratio (FR), which represented the estimated severity of the impact load with respect to the load bearing capacity of the femur.

A second parameter was designed to weight the fragility ratio according to the subject's probability of falling on the hip, based on self-reported fall frequency (FF) measured at baseline. Fall frequency information was available from questionnaires that recorded the number of falls in the year prior to subject intake, according to the subject. This weighted parameter was termed expected endpoint value (EEV) and was expressed using the following formulas:

$$EEV = FR * P_{fall} \quad (1)$$

$$P_{fall} = 1 - (1 - P_{hip})^{N * FF} \quad (2)$$

where P_{fall} is the probability of the subject falling at least once on the greater trochanter over a period of N years, and P_{hip} is the probability of a given fall impacting the hip. For the present study, N was fixed to 5 years, in order to represent the follow-up period of the AGES cohort, and P_{hip} was estimated at 40%, based on observational studies of fall characteristics [46]. A minimum fall frequency of one fall every five years was assumed for subjects that did not report any falls at baseline (FF = 0.2).

Simulated strains of the surface elements within the femoral neck of the non-linear proximal femur model were also tested as potential hip fracture predictors. Femoral neck elements were selected within a spherical volume of interest (VOI) centered at the anatomical center of the femoral neck, defined using an in-house landmarking program

(Appendix A). The radius of the sphere was equal to the radius of the femoral head scaled by a factor of 1.25. For surface elements within this VOI, the maximum first principal strain, minimum third principal strain, and maximum and minimum volumetric strains were measured at the time point of ultimate femur force. The change in these four parameters was also measured between the time of ultimate force, and the time point beyond ultimate force, at which the femur force had decreased to 90% of the ultimate force. Additionally, the overall maximum principal strain and minimum principal strain within the femur during the entire time length of the simulation was measured, as well as the number of elements that reached a volumetric strain above 3.0, 3.5, 4.0, 4.5, and 5.0%. Thus, 15 different surface strain measurements were derived from each model, however due to the similar performance of the different strain metrics, only the results for change in maximum volumetric strain (ΔMVS) are reported here for brevity. Finally, expected endpoint values for both ΔMVS (EEVS) and aBMD (EEVD) were calculated using Eq. (1), by replacing the fragility ratio with each parameter, respectively, in order to test the effect of weighting these predictors based on the subject's risk of falling.

Age-adjusted logistic regression models for classifying subject fracture status were calculated using both FEA based predictions and total femur aBMD using Bayesian inference within the PyMC3 statistical package [47]. Area under the receiver-operator characteristic curve (AUC) was used to compare the diagnostic performance of each logistic regression model. In the event of the ROC curves crossing, which would frustrate inference from AUC calculations, partial AUC was also calculated for a defined specificity range, specifically from 100% specificity to the specificity corresponding to the aBMD threshold for osteoporosis in Caucasian men and women (0.64 g/cm^2) [48]. Limiting the AUC calculations in this manner provided a comparison of the sensitivity between FE and aBMD based prediction models, while focusing on the subjects at highest risk. Probabilistic differences between aBMD and FEA based AUC measurements were tested using Monte Carlo confidence interval estimates [49] based on 100,000 random samples from a Gaussian kernel density estimate that was derived for each classifier using the probability scores from each logistic regression model. The corresponding p-values indicated whether differences in AUC results were statistically different from zero ($p < 0.05$). An additional logistic regression was performed for each FEA-based predictor that was adjusted for both age and aBMD, in order test whether FEA parameters were still significantly associated with fracture classification after accounting for the subject's aBMD.

2.4.2. Alternative analysis

The limitations of self-reported fall-frequency have been well documented in scientific literature [50–52]. Therefore, an alternative analysis was performed to eliminate the confounding effect of fall frequency uncertainty by excluding subjects that did not report falling, which are challenging to classify correctly using mechanical or densitometric predictors. From the 254 subjects tested, a subgroup was selected that only included subjects that either reported falling in the year prior to baseline, but did not fracture (27 controls), or sustained a hip fracture within the follow up period, which was likely due to a fall (95 cases). This subset was equivalent to knowing a priori whether a subject fell and suffered a fracture or if the subject was a frequent faller but did not fracture. Age-adjusted logistic regression was repeated for aBMD, FR, and ΔMVS using this subgroup, and significant differences in total AUC between aBMD and FEA-based classifiers was again tested using Monte Carlo confidence interval estimates. Partial AUC could not be computed for this scenario, because none of the control subjects had aBMD corresponding to osteoporosis, and therefore a corresponding specificity cutoff could not be determined.

2.4.3. Predicting subject-specific femur impact forces

A linear regression model was calculated in R (Core Team, v3.0.2, 2013, Vienna) that predicted the ultimate force measured at the contact between femoral head and acetabular cup based on the elastic simulations (F_{femur}), as a function of all the subject-specific parameters, including age, height, weight, BMI, total aBMD, fall inertia, femur head radius, pelvis width, and soft tissue thickness. Afterwards, the backward step function within R was applied to optimize the regression by systematically reducing the parameters in the model until a combination was found that explains the most variation in subject-specific ultimate femur force. The purpose of this test was to describe the variance in subject-specific femur loads explained by parameters that were external to the FE model of the femur itself. A force reduction factor (η) was defined for each subject as the ratio between F_{femur} and the ultimate force measured at the contact between the floor and the subject's soft tissue. A linear regression model was subsequently calculated to measure the variance in η explained by the subject's undeformed soft tissue thickness at the greater trochanter (T_{ST}).

3. Results

3.1. Fracture classification and statistical analysis

Examples of femur impact forces within simulations indicating high and low fragility ratios are presented in Fig. 3. The femur force in nonlinear simulations with high FR (i.e. > 1.3) typically included failure behavior in the form of a steep force drop due to tensile damage in the inferior femoral neck. This predominantly occurred within elements in the basi-cervical region that represented bone densities near the transition from cortical to trabecular material properties (Fig. 4).

A summary of the blinded comparison of the different hip fracture classification models to the hip fracture registry analysis for all subjects tested (95 cases, 159 controls) is presented in Table 3. The corresponding ROC curves and AUC probability densities are depicted in Fig. 5. Histograms detailing the distribution of probability scores from each logistic regression are compared between fracture and non-fracture groups in Fig. 6. All FEA-based hip fracture classifiers remained significant in the logistic regression models after adjusting for both age and aBMD ($p < 0.05$). Total AUC was highest for EEVS (0.73), followed by ΔMVS (0.72), FR (0.71), aBMD (0.70), EEV (0.67), and EEVD (0.629). Partial-AUC was highest for FR (0.107), and followed by EEVS (0.105), ΔMVS (0.098), EEV (0.098), aBMD (0.094), and EEVD (0.069). Monte Carlo simulations indicated that none of the FEA-based hip fracture classifiers were significantly different from aBMD, with respect to the measured AUC values.

3.2. Alternative analysis

A summary of the blinded hip fracture classification analysis for subjects that either reported falling within twelve months prior to baseline, or sustained a hip fracture (95 cases, 27 controls) is presented in Table 4. The corresponding ROC curves and AUC probability densities for the faller-only analysis are depicted in Fig. 7. Histograms detailing the distribution of probability scores from the faller-only logistic regressions are compared between fracture and non-fracture groups in Fig. 8. Total AUC was highest for ΔMVS (0.85), followed by FR (0.76), and aBMD (0.74). Monte Carlo simulations indicated that AUC of the classification model based on ΔMVS was significantly different from aBMD ($p < 0.05$).

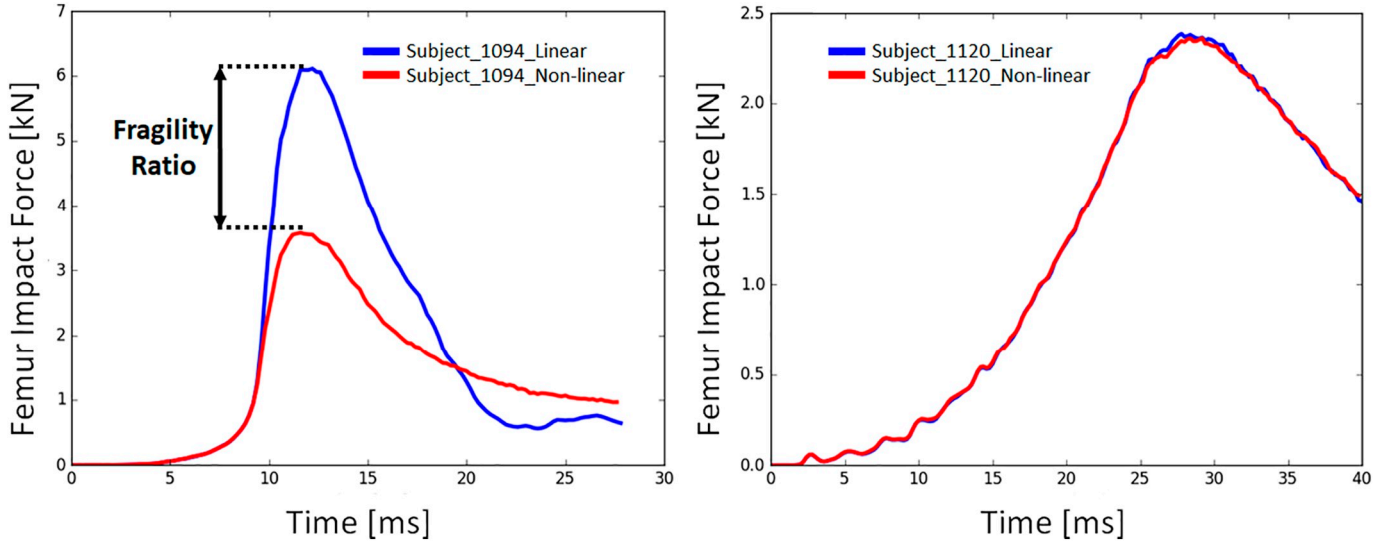

Fig. 3. Examples of femur impact forces vs time for a subject with high fragility ratio (left) and low fragility ratio (right). The red curve denotes a biofidelic model with non-linear stress-strain relationships within the femur properties, and the blue curve denotes an identical model with linear elastic stress-strain relationships femur. (For interpretation of the references to colour in this figure legend, the reader is referred to the web version of this article.)

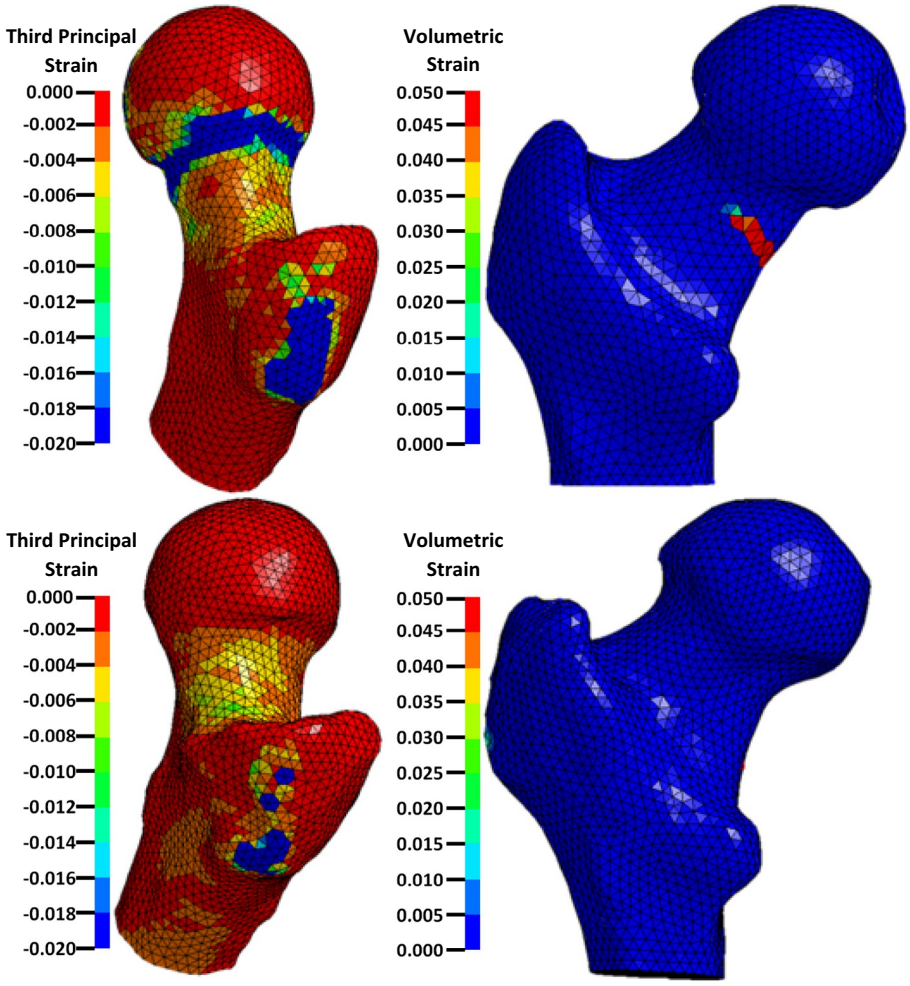

Fig. 4. Distribution of third principal strains (left) and volumetric strains (right) on the surface of the proximal femur, for a subject with high FR (2.0, top), and low FR (1.0, bottom) at the point of peak force between the femur and acetabulum.

Table 3
Fracture classification performance for aBMD and FEA-based predictors for all subjects tested (95 cases, 159 controls).

	Total AUC	Partial AUC	AUC comparison (p-value)	aBMD-adjusted regression (p-value)
aBMD	0.699	0.094	–	–
FR	0.712	0.107	0.43	0.003
ΔMVS	0.717	0.098	0.30	< 0.001
EEV	0.682	0.098	0.75	0.006
EEVS	0.727	0.105	0.25	< 0.001
EEVD	0.629	0.069	–	–

3.3. Predicting subject-specific femur force

Backwards elimination of the multivariable linear regression model predicting ultimate femur impact force at the femur-acetabulum contact in elastic models (F_{femur}) as a function of the available subject-specific parameters, returned following formula the best captured the variance within the simulations ($R^2 = 0.79$; RMSE = 0.46 kN):

$$F_{femur} = 86 \cdot R_{FH} + 43 \cdot W_P - 52 \cdot T_{ST} - 1230 \text{ [N]}$$

where R_{FH} is femoral head radius ($p < 0.005$), W_P is the pelvis width ($p \ll 0.001$), and T_{ST} is the soft tissue thickness ($p \ll 0.001$), all measured in millimeters. Subject-specific force reduction factor (η) was correlated with soft tissue thickness according to the following equation ($R^2 = 0.76$):

$$\eta = -5.2 \cdot 10^{-3} \cdot T_{ST} + 0.88 \text{ [–]}$$

4. Discussion

The aim of this study was to test whether biofidelic simulations of hip impact during sideways falling can accurately classify the incidence of hip fracture, retrospectively for elderly women. To test this hypothesis, the sensitivity and specificity of fracture classification models based on the fragility ratio and change in volumetric strain at the surface of the femoral neck were compared to prediction models based on total femur aBMD measurements. An alternative analysis also compared hip fracture classification models only for subjects that reported a history of falling or suffered actual hip fracture. An additional aim of this study was to predict the load sustained by the femur during impact as a function of subject anthropometrics in order to quantify subject-specific fall severity. The total and partial AUC of the classification models based on fragility ratio, and change in surface strain on the femoral neck, were higher than models based on aBMD, however the differences were not deemed statistically significant. Weighting these parameters according to the estimated fall probability, based on self-reported fall frequency, did not significantly improve classification performance. However, when non-fallers were excluded from the analysis, thus artificially removing the effect of fall risk uncertainty, the AUC of the classification model based on maximum change in surface strain became significantly different from the model based on total femur aBMD. Finally, the majority of the variance in femur impact force could be explained as a function of the femoral head radius, pelvis width, and soft tissue thickness.

The difference in sensitivity of FEA-based predictors compared to aBMD measurements was comparable to a similar retrospective study of different clinical data [16], however the statistical significance of these prediction models could not be compared. Previous FEA studies of elderly women from the AGES-Reykjavik cohort reported mixed results; one study used logistic regression to predict fracture status (binary) as a function of FEA-based femoral strength and reported that strength remained significantly associated with the regression model after adjusting for both age and aBMD [14]. Conversely, another study used multiple linear regression to model femoral strength as a function hip fracture status, age, weight, and height, and reported that fracture status in women was no longer significantly associated with femoral strength after the model was adjusted for aBMD [15]. In comparison, the FEA-based hip fracture predictors in the present study significantly improved every logistic regression model after adjusting for age and total femur aBMD. A previous retrospective study also estimated subject-specific load-to-strength ratio, by estimating loads using theoretical three-link models of sideways falling [42], but this parameter failed to outperform aBMD and FEA-based femur strength measurements [14]. In contrast, the biofidelic models in the present study directly simulated subject-specific loads, which included the attenuation of impact force between the ground and femur provided by the soft tissue.

There is ample evidence that hip fractures are strongly associated with falling [1,2,53]; it was therefore surprising that weighting the FEA parameters based on fall frequency did not improve the performance of the majority of classification models. Closer inspection of the fall frequency data revealed that only 20% of subjects tested in this study reported falling within the 12 months prior to baseline. For comparison, another longitudinal study involving a cohort of 887 elderly women reported that 64% of subjects sustained a fall within the 1.6 year monitoring period [17]. Combined with the known weaknesses of self-reported fall data [50–52], this finding could explain why significant differences between FEA and aBMD predictors were only detected once subjects that did not report falling were excluded. Although these

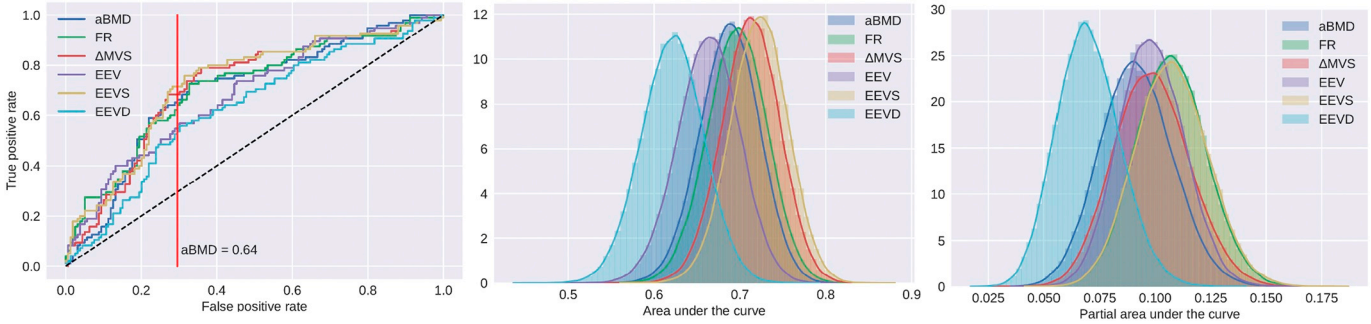

Fig. 5. ROC curves (left) of FR, ΔMVS, EEV, EEVS, aBMD, and EEVD for all subjects tested (95 cases, 159 controls). The specificity of the aBMD-based osteoporosis threshold is indicated as a vertical red line, which was used to calculate partial-AUC. Corresponding probability distributions for total AUC (center) and partial AUC (right). (For interpretation of the references to colour in this figure legend, the reader is referred to the web version of this article.)

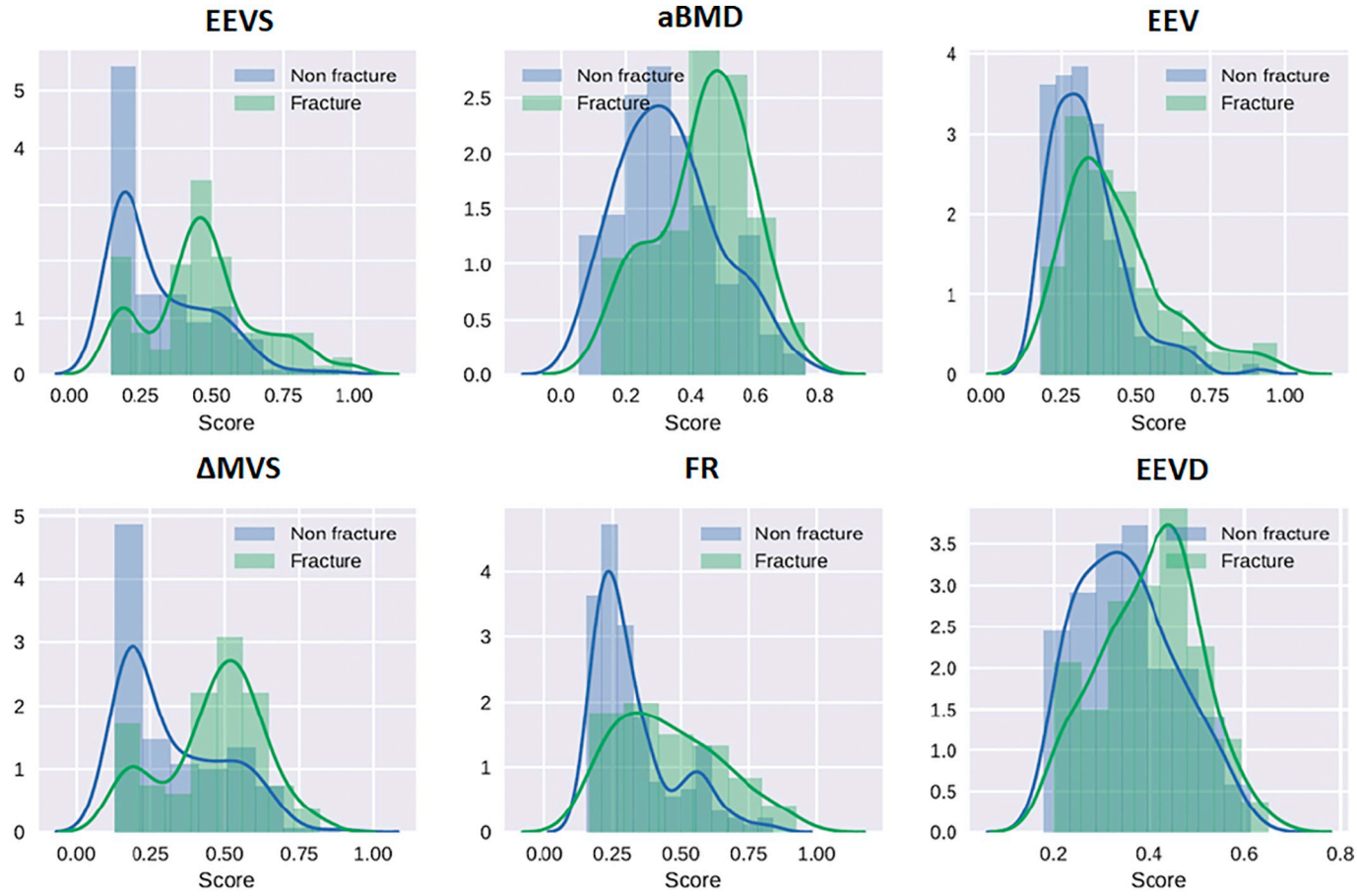

Fig. 6. Histograms and probability density curves of the logistic regression score for all 254 subjects tested (95 cases, 159 controls), for six predictor variables: Expected end-point value based on change in max volumetric strain (EEVS; top left), areal bone mineral density (aBMD; top center), expected end-point value based on fragility ratio (EEV; top right), change in max volumetric strain (ΔMVS; bottom left), fragility ratio (FR; bottom center), and expected end-point value based on areal bone mineral density (EEVD; bottom right).

Table 4
Fracture classification performance for aBMD and FEA-based predictors tested only on subjects that reported falling within twelve months prior to baseline, or sustained hip fracture (95 cases, 27 controls). Values in bold indicate statistical significance.

	Total AUC	AUC comparison (p-value)	aBMD-adjusted regression (p-value)
aBMD	0.74	–	–
FR	0.76	0.21	0.006
ΔMVS	0.85	**< 0.05**	< 0.001

criteria reduced the number of control subjects and is unrealistic as a screening method since the selection was based on posterior knowledge of fracture status, this result suggests that attaining an AUC > 0.8 for classifying hip fracture may require a better assessment of fall risk, fall orientation, and protective responses [54].

This was the first study to perform a retrospective analysis of clinical data to predict the ultimate impact force on the femur using dynamic simulations, while including models of the pelvis and soft tissue. The backwards step function in R indicated that a model based solely on pelvis and soft tissue anatomy was able to explain the most variance in femur impact force. This does not imply, however, that height and weight do not influence the impact force, since these parameters are also correlated with pelvis and soft tissue dimensions. This optimized regression model indicates that subject-specific femur loads are sensitive to parameters external to the femur model itself, highlighting an important advantage of a more biofidelic modeling approach, which incorporates more subject-specific boundary conditions for the femur. These findings are also in alignment with another dynamic FEA study of hip impact that reported a significant correlation between soft tissue thickness and ultimate impact force at the floor, where body height and weight were similarly not correlated with impact force [55]. The correlation between the force reduction factor and soft tissue thickness in present study is in line with findings from previously published studies [43,56–59], which strongly suggests that soft tissue thickness is a determining factor of hip fracture due to falling.

The FE modeling technique presented in this study is not a perfect anatomical representation of the subject, and thus certain pieces of subject-specific information are still lacking that could potential increase the sensitivity of the model to fracture status. The impact velocity was fixed at 3 m/s for all subjects, however this parameter likely

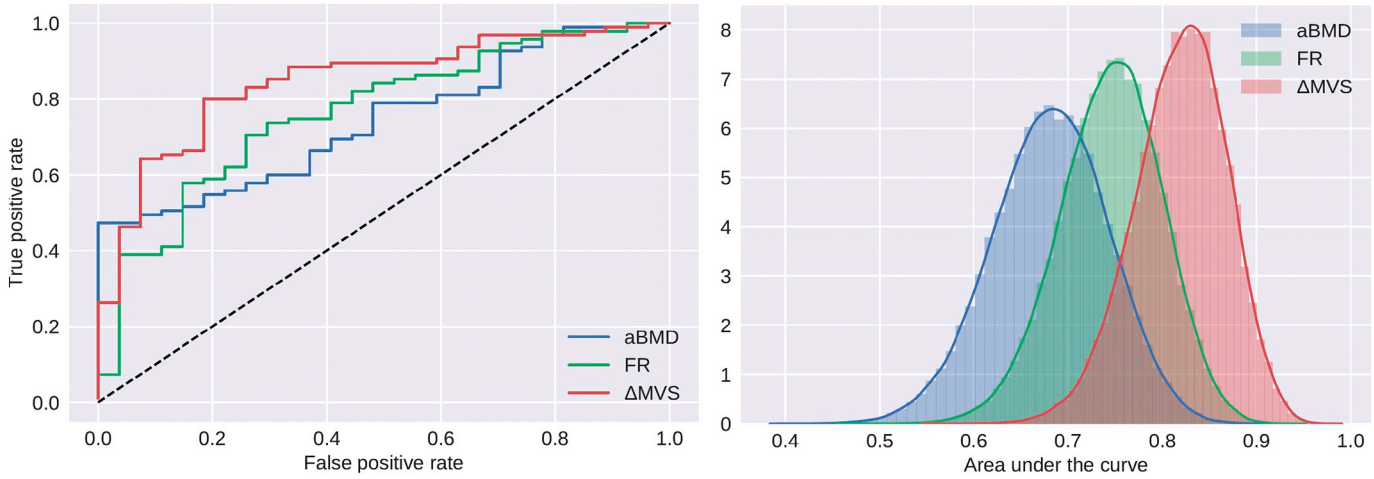

Fig. 7. ROC curves (left) of FR, ΔMVS, and aBMD, only for subjects that either reported falling within twelve months prior to baseline, or sustained a hip fracture (95 cases, 27 controls). Corresponding probability distributions for total AUC (right).

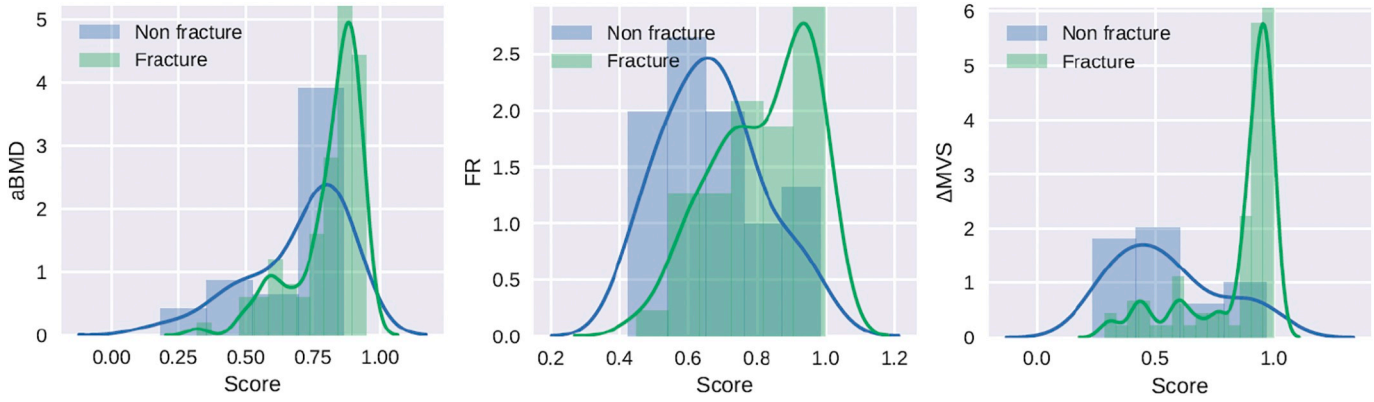

Fig. 8. Histograms and probability density curves of the logistic regression score only for subjects that either reported falling within twelve months prior to baseline, or sustained a hip fracture (95 cases, 27 controls).

depends on subject anthropometrics, and could therefore affect the sensitivity of the biofidelic models. The soft tissue properties were chosen to reflect a blend between muscle and fat, but this ratio could also change based on age and lifestyle. The biofidelity of the model could potentially be improved by modeling subject-specific soft tissue shapes, however the subjects were lying down within the CT scanner effectively distorted the shape of the soft tissue around the hip, making it less representative of a real fall. Future cohort studies concerning hip fracture should therefore consider including a three-dimensional body surface scan, with the subject in a standing position, as was performed in the SizeUSA database utilized by this study. The role of active versus passive muscle contraction could also influence the proportion of impact energy transmitted directly to the femur, by making the entire structure more rigid. Finally, the AUC for aBMD was higher than other cross-sectional studies [60]. A possible explanation is that the aBMD measurements in the present study were based on 2D projections from 3D QCT scans as a surrogate for DXA. This could affect the accuracy of the hip fracture classification model based on aBMD, because an areal measurement of density is sensitive to the projection angle, which is better controlled in a projected QCT scan than a clinical DXA evaluation, where measurements can vary from six to 15% for the same patient [61].

The fall alignment within the biofidelic models represents the posterior-lateral impact scenario, which has been described as the most severe in terms of ultimate impact load on the proximal femur [15,16,40]. While this critical alignment is likely true on average for the population, it does not effectively describe the size of the envelope of all possible fall alignments that could be proportional to an individual's likelihood of fracture. The lack of subject-specific femur anteversion, due to the limited field of view in the CT scans, could also affect subject-specific fall alignment, as well as the definition of the femur coordinate system. The present study overcame this limitation by using an automated measurement of the femoral neck center to define the anterior plane of the femur, which differed from the ISB convention that relies on landmarks on the surface of the femoral condyles. Future studies will require either full femur CT scans or more robust statistical

shape models of distal femur geometry in order to eliminate this limitation.

5. Conclusions

This study has demonstrated that biofidelic FE simulations provide unique information regarding hip fracture mechanics resulting from sideways falls. A novel assessment combining information from FEA parameters and fall probability revealed the confounding role of fall frequency in the evaluation of different hip fracture classification models. When the effect of fall risk uncertainty was reduced by excluding non-fallers from the analysis using posterior knowledge of fracture incidents, a statistically significant difference was detected between aBMD and FEA performance. While an analysis based on such posterior knowledge is unsuitable for developing new screening techniques, it suggests that understanding fall risk is an important limitation that must be overcome before different fracture risk predictors can be effectively compared. Finally, a novel estimation of subject-specific loading of the proximal femur during a sideways fall was quantified from the biofidelic models. Looking forward, the technology for generating biofidelic models could serve as a future platform for testing additional subject-specific information in attempt to further enhance the performance of retrospective hip fracture classification. Finally, combining the modeling techniques developed in this study with new cohort data specifically tailored to characterize the risk factors of hip fracture, including improved measurements of fall probability and soft tissue properties, would provide a powerful research tool for identifying individuals predisposed to hip fracture.

Conflict of interest

The authors have no conflicts of interest related to this work.

Acknowledgements

This study was funded by the Swiss National Science Foundation (Project no. 205321_144435), the ETH-Foundation (grant no. ETH1514-1), and the St. Josef's Hospital Fund, Reykjavik, Iceland.

Appendix A. Fall alignment of the biofidelic hip impact model

A graphical representation of the landmarking algorithm is provided in Fig. A1. The femur head center and radius were measured by identifying a corresponding sphere location and radius using the Hough transform. The sphere corresponding to femoral head radius was scaled by a factor of 1.2 so that this larger sphere would intersect with the surface of the femoral neck. The center of the ellipsoidal shape defined by the line of intersection between the enlarged sphere and the bone surface defined the center of the femoral neck. The spherical centers of the left and right femoral condyles were also identified using the Hough transform, and the mid-condyle point was defined midway between the condyle centers. Finally, the superior tip of the greater trochanter was defined as the most distal surface point from the mid-condyle point, excluding the femoral head.

Pelvis and femur coordinate systems and subsequent rotations are depicted in Fig. A2. The femur coordinate system was defined with an origin at the femoral head center. The femoral shaft axis was defined between the superior tip of the greater trochanter and the mid condyle point. The femoral neck axis was defined as a vector orthogonal to the femoral shaft axis, but in plane with the femoral neck center. The pelvis coordinate system was defined with the origin at femoral head center of the native left femur. The pelvic width axis was defined as the vector between the left and right femoral head centers. The pelvic depth axis was defined as the vector between the center of superior surface of the S1 vertebra and the midpoint of the pelvic width axis.

The fall alignment of the femur and pelvis was defined by initially aligning the pelvic width axis parallel to the gravitational vector (i.e. global X). The femoral shaft axis was then aligned parallel to the pelvic depth axis orthogonal to the gravitational vector (i.e. global Y), such that the normal vector of the plane defined by the femoral head, neck, and mid-condyle points was orthogonal to the gravitational vector. The femurs were rotated 35° in hip flexion based on fall kinematics from experiments [41], and internally rotated 5° to prevent the femur from deflecting away from the acetabulum through external rotation. Finally, the femur was adducted 10° to prevent the knee from contacting the ground. The pelvis was tilted posteriorly 12° around the pelvic width axis [62], and rotated 15° around a vector with an origin at the femoral head center, oriented orthogonal to the pelvic gravitational axis and femoral shaft axis (i.e. global Z).

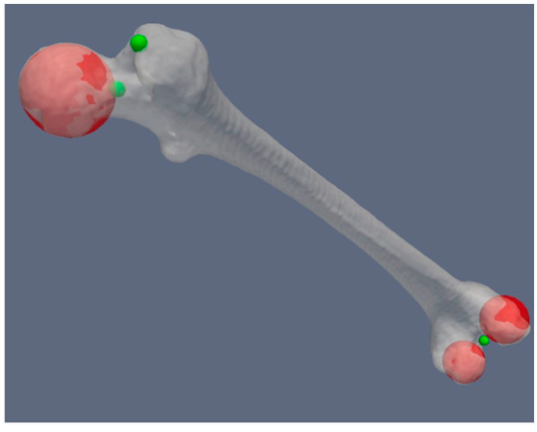

Fig. A1. Depiction of automated landmarking algorithm and representative spheres calculated using the Hough transform (red), and subsequent definition of the anatomical femoral neck center, greater trochanter, and mid-condyle point (green).

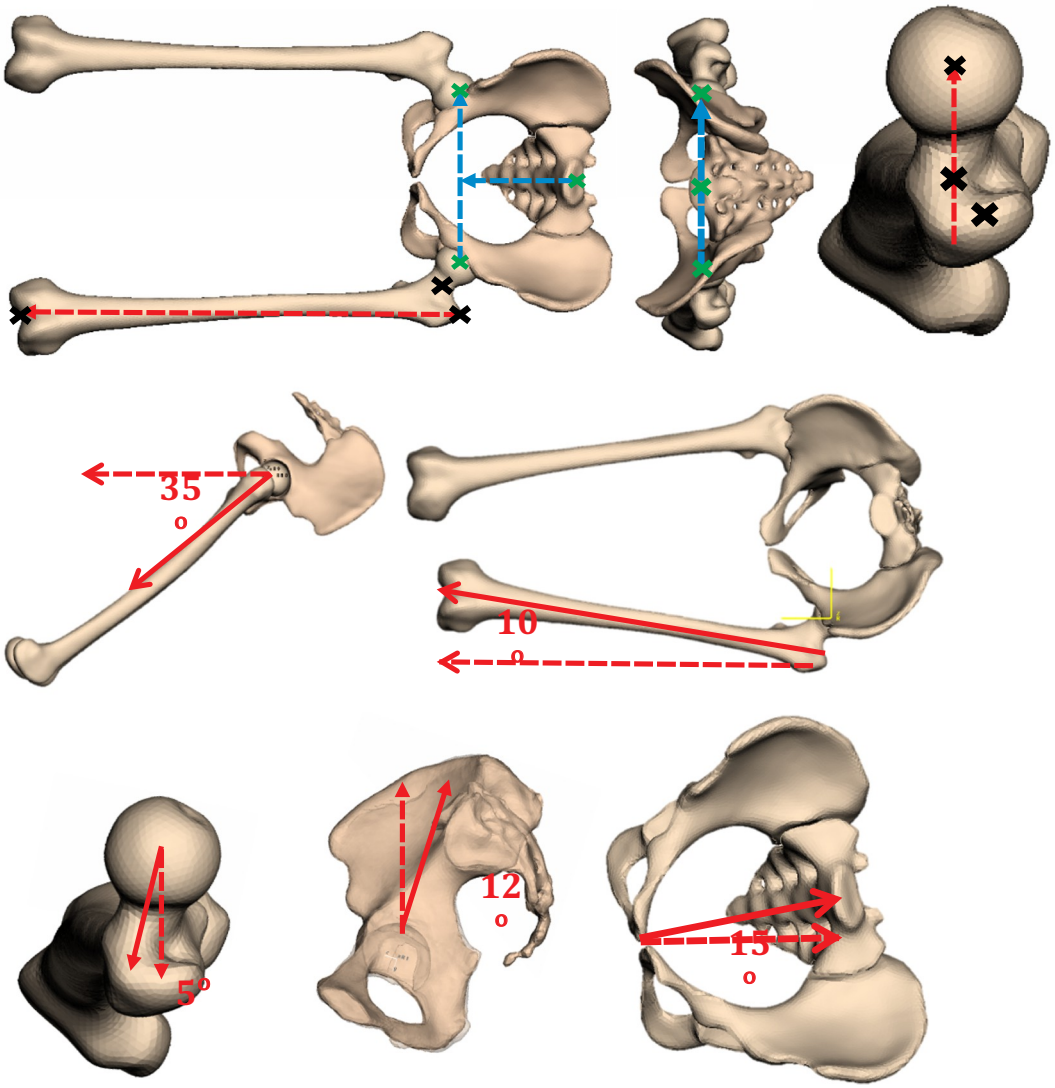

Fig. A2. The landmarks used to define the coordinate systems of the pelvis and femurs (top), with bones aligned square to the global coordinate system (i.e. non-anatomical). Transforms from the initial alignment into fall alignment included hip flexion (middle left), hip adduction (middle right), internal rotation of the hip (bottom left), pelvic tilt (bottom center), and pelvic rotation relative to the ground (bottom right).

References

[1] J. Parkkari, P. Kannus, M. Palvanen, A. Natri, J. Vainio, H. Aho, et al., Majority of hip fractures occur as a result of a fall and impact on the greater trochanter of the femur: a prospective controlled hip fracture study with 206 consecutive patients, Calcif. Tissue Int. 65 (1999) 183–187.

[2] W. Hayes, E. Myers, S. Robinovitch, A. Van Den Kroonenberg, A. Courtney, T. McMahon, Etiology and prevention of age-related hip fractures, Bone 18 (1996) S77–S86.

[3] T. Nevalainen, L.A. Hiltunen, P. Jalovaara, et al., Functional ability after hip fracture among patients home-dwelling at the time of fracture, Cent. Eur. J. Public Health 12 (2004) 211–216.

[4] W. Ekström, R. Miedel, S. Ponzer, M. Hedström, E. Samnegård, J. Tidermark, Quality of life after a stable trochanteric fracture—a prospective cohort study on 148 patients, J. Orthop. Trauma 23 (2009) 39–44.

[5] S. Haleem, L. Lutchman, R. Mayahi, J. Grice, M. Parker, Mortality following hip fracture: trends and geographical variations over the last 40 years, Injury 39 (2008) 1157–1163.

[6] E. Hernlund, A. Svedbom, M. Ivergård, J. Compston, C. Cooper, J. Stenmark, et al., Osteoporosis in the European Union: medical management, epidemiology and economic burden, Arch. Osteoporos. 8 (2013) 136.

[7] T.L. Järvinen, H. Sievänen, K.M. Khan, A. Heinonen, P. Kannus, Shifting the focus in fracture prevention from osteoporosis to falls, Br. Med. J. 336 (2008) 124.

[8] K.L. Stone, D.G. Seeley, L.-Y. Lui, J.A. Cauley, K. Ensrud, W.S. Browner, et al., BMD at multiple sites and risk of fracture of multiple types: long-term results from the Study of Osteoporotic Fractures, J. Bone Miner. Res. 18 (2003) 1947–1954.

[9] S.A. Wainwright, L.M. Marshall, K.E. Ensrud, J.A. Cauley, D.M. Black, T.A. Hillier, et al., Hip fracture in women without osteoporosis, J. Clin. Endocrinol. Metab. 90 (2005) 2787–2793.

[10] S.C.E. Schuit, M. van der Klift, A.E.A.M. Weel, C.E.D.H. de Laet, H. Burger, E. Seeman, et al., Fracture incidence and association with bone mineral density in elderly men and women: the Rotterdam Study, Bone 34 (2004) 195–202.

[11] J.E. Koivumäki, J. Thevenot, P. Pulkkinen, V. Kuhn, T.M. Link, F. Eckstein, et al., Ct-based finite element models can be used to estimate experimentally measured failure loads in the proximal femur, Bone 50 (2012) 824–829.

[12] D. Dragomir-Daescu, J.O. Den Buijs, S. McEligot, Y. Dai, R.C. Entwistle, C. Salas, et al., Robust QCT/FEA models of proximal femur stiffness and fracture load during a sideways fall on the hip, Ann. Biomed. Eng. 39 (2011) 742–755.

[13] L. Grassi, E. Schileo, F. Taddei, L. Zani, M. Juszczyk, L. Cristofolini, et al., Accuracy of finite element predictions in sideways load configurations for the proximal human femur, J. Biomech. 45 (2012) 394–399.

[14] D.L. Kopperdahl, T. Aspelund, P.F. Hoffmann, S. Sigurdsson, K. Siggeirsdottir, T.B. Harris, et al., Assessment of incident spine and hip fractures in women and men using finite element analysis of CT scans, J. Bone Miner. Res. 29 (2014) 570–580.

[15] J. Keyak, S. Sigurdsson, G. Karlsdottir, D. Oskarsdottir, A. Sigmarsdottir, J. Kornak, et al., Effect of finite element model loading condition on fracture risk assessment in men and women: the AGES-Reykjavik study, Bone 57 (2013) 18–29.

[16] M. Qasim, G. Farinella, J. Zhang, X. Li, L. Yang, R. Eastell, et al., Patient-specific finite element estimated femur strength as a predictor of the risk of hip fracture: the effect of methodological determinants, Osteoporos. Int. 27 (2016) 2815–2822.

[17] K. Sanders, K. Lim, A. Stuart, A. Macleod, D. Scott, G. Nicholson, et al., Diversity in fall characteristics hampers effective prevention: the precipitants, the environment, the fall and the injury, Osteoporos. Int. (2017) 1–11.

[18] N.M. Nachreiner, M.J. Findorff, J.F. Wyman, T.C. McCarthy, Circumstances and consequences of falls in community-dwelling older women, J. Women's Health 16 (2007) 1437–1446.
[19] M.C. Nevitt, S.R. Cummings, S. Kidd, D. Black, Risk factors for recurrent non-syncopal falls: a prospective study, JAMA 261 (1989) 2663–2668.
[20] W. Enns-Bray, H. Bahaloo, I. Fleps, O. Ariza, S. Gilchrist, R. Widmer, et al., Material mapping strategy to improve the predicted response of the proximal femur to a sideways fall impact, J. Mech. Behav. Biomed. Mater. 78 (2018) 196–205.
[21] H. Bahaloo, W. Enns-Bray, I. Fleps, O. Ariza, S. Gilchrist, R.W. Soyka, et al., On the failure initiation in the proximal human femur under simulated sideways Fall, Ann. Biomed. Eng. 46 (2018) 270–283.
[22] O. Ariza, S. Gilchrist, R. Widmer, P. Guy, S. Ferguson, P. Cripton, et al., Comparison of explicit finite element and mechanical simulation of the proximal femur during dynamic drop-tower testing, J. Biomech. 48 (2015) 224–232.
[23] B. Helgason, S. Gilchrist, O. Ariza, J. Chak, G. Zheng, R. Widmer, et al., Development of a balanced experimental-computational approach to understanding the mechanics of proximal femur fractures, Med. Eng. Phys. 36 (2014) 793–799.
[24] S. Gilchrist, K. Nishiyama, P. de Bakker, P. Guy, S. Boyd, T. Oxland, et al., Proximal femur elastic behaviour is the same in impact and constant displacement rate fall simulation, J. Biomech. 47 (2014) 3744–3749.
[25] I. Fleps, W. Enns-Bray, P. Guy, S.J. Ferguson, P.A. Cripton, B. Helgason, On the internal reaction forces, energy absorption, and fracture in the hip during simulated sideways fall impact, PLoS One 13 (8) (2018) e0200952.
[26] T.B. Harris, L.J. Launer, G. Eiriksdottir, O. Kjartansson, P.V. Jonsson, G. Sigurdsson, et al., Age, gene/environment susceptibility-Reykjavik Study: multidisciplinary applied phenomics, Am. J. Epidemiol. 165 (2007) 1076–1087.
[27] J. Keyak, S. Sigurdsson, G. Karlsdottir, D. Oskarsdottir, A. Sigmarsdottir, S. Zhao, et al., Male-female differences in the association between incident hip fracture and proximal femoral strength: a finite element analysis study, Bone 48 (2011) 1239–1245.
[28] G. Sigurdsson, T. Aspelund, M. Chang, B. Jonsdottir, S. Sigurdsson, G. Eiriksdottir, et al., Increasing sex difference in bone strength in old age: the age, gene/environment susceptibility-Reykjavik study (AGES-REYKJAVIK), Bone 39 (2006) 644–651.
[29] Y. Pauchard, T. Fitze, D. Browarnik, A. Eskandari, I. Pauchard, W. Enns-Bray, et al., Interactive graph-cut segmentation for fast creation of finite element models from clinical ct data for hip fracture prediction, Comput. Methods Biomech. Biomed. Engin. 19 (2016) 1693–1703.
[30] L.V. Burgin, L. Edelsten, R.M. Aspden, The mechanical and material properties of elderly human articular cartilage subject to impact and slow loading, Med. Eng. Phys. 36 (2014) 226–232, https://doi.org/10.1016/j.medengphy.2013.11.002.
[31] Z. Li, J.-E. Kim, J.S. Davidson, B.S. Etheridge, J.E. Alonso, A.W. Eberhardt, Biomechanical response of the pubic symphysis in lateral pelvic impacts: a finite element study, J. Biomech. 40 (2007) 2758–2766.
[32] N. Hammer, H. Steinke, U. Lingslebe, I. Bechmann, C. Josten, V. Slowik, et al., Ligamentous influence in pelvic load distribution, Spine J. 13 (2013) 1321–1330, https://doi.org/10.1016/j.spinee.2013.03.050.
[33] B. Helgason, S. Gilchrist, O. Ariza, P. Vogt, W. Enns-Bray, R. Widmer, et al., The influence of the modulus-density relationship and the material mapping method on the simulated mechanical response of the proximal femur in side-ways fall loading configuration, Med. Eng. Phys. 38 (2016) 679–689.
[34] E. Schileo, E. Dall'Ara, F. Taddei, A. Malandrino, T. Schotkamp, M. Baleani, et al., An accurate estimation of bone density improves the accuracy of subject-specific finite element models, J. Biomech. 41 (2008) 2483–2491.
[35] E.F. Morgan, H.H. Bayraktar, T.M. Keaveny, Trabecular bone modulus-density relationships depend on anatomic site, J. Biomech. 36 (2003) 897–904.
[36] B. Helgason, F. Taddei, H. Pálsson, E. Schileo, L. Cristofolini, M. Viceconti, et al., A modified method for assigning material properties to FE models of bones, Med. Eng. Phys. 30 (2008) 444–453.
[37] W.T. Dempster, G.R.L. Gaughran, Properties of body segments based on size and weight, Am. J. Anat. 120 (1967) 33–54.
[38] T. Albrecht, M. Lüthi, T. Gerig, T. Vetter, Posterior shape models, Med. Image Anal. 17 (2013) 959–973, https://doi.org/10.1016/j.media.2013.05.010.
[39] E. Taghizadeh, M. Kistler, P. Büchler, M. Reyes, Fast prediction of femoral biomechanics using supervised machine learning and statistical shape modeling, Computational Biomechanics for Medicine, Springer, 2016, pp. 107–116.
[40] R.D. Carpenter, G.S. Beaupré, T.F. Lang, E.S. Orwoll, D.R. Carter, New QCT analysis approach shows the importance of fall orientation on femoral neck strength, J. Bone Miner. Res. 20 (2005) 1533–1542.
[41] A.J. van den Kroonenberg, W.C. Hayes, T.A. McMahon, Hip impact velocities and body configurations for voluntary falls from standing height, J. Biomech. 29 (1996) 807–811.
[42] A. van den Kroonenberg, T. McMahon, W. Hayes, Dynamic models for sideways falls from standing height, J. Biomech. Eng. 117 (1995) 309–318.
[43] Y. Luo, M. Nasiri Sarvi, P. Sun, W.D. Leslie, J. Ouyang, Prediction of impact force in sideways fall by image-based subject-specific dynamics model, Int. Biomech. 1 (2014) 1–14.
[44] A.C. Laing, S.N. Robinovitch, Characterizing the effective stiffness of the pelvis during sideways falls on the hip, J. Biomech. 43 (2010) 1898–1904.
[45] S.N. Robinovitch, W.C. Hayes, T.A. McMahon, Distribution of contact force during impact to the hip, Ann. Biomed. Eng. 25 (1997) 499–508.
[46] Y. Yang, D. Mackey, T. Liu-Ambrose, F. Feldman, S. Robinovitch, Risk factors for hip impact during real-life falls captured on video in long-term care, Osteoporos. Int. 27 (2016) 537–547.
[47] J. Salvatier, T.V. Wiecki, C. Fonnesbeck, Probabilistic programming in Python using PyMC3, PeerJ Comput. Sci. 2 (2016) e55.
[48] A.C. Looker, E.S. Orwoll, C.C. Johnston, R.L. Lindsay, H.W. Wahner, W.L. Dunn, et al., Prevalence of low femoral bone density in older U.S. adults from NHANES III, J. Bone Miner. Res. 12 (1997) 1761–1768.
[49] K.J. Preacher, J.P. Selig, Advantages of Monte Carlo confidence intervals for indirect effects, Commun. Methods Meas. 6 (2012) 77–98.
[50] S.N. Robinovitch, F. Feldman, Y. Yang, R. Schonnop, P.M. Leung, T. Sarraf, et al., Video capture of the circumstances of falls in elderly people residing in long-term care: an observational study, Lancet 381 (2013) 47–54.
[51] A.C. Grundstrom, C.E. Guse, P.M. Layde, Risk factors for falls and fall-related injuries in adults 85 years of age and older, Arch. Gerontol. Geriatr. 54 (2012) 421–428.
[52] A.J. Campbell, M.J. Borrie, G.F. Spears, Risk factors for falls in a community-based prospective study of people 70 years and older, J. Gerontol. 44 (1989) M112–M117.
[53] P. Geusens, P. Autier, S. Boonen, J. Vanhoof, K. Declerck, J. Raus, The relationship among history of falls, osteoporosis, and fractures in postmenopausal women, Arch. Phys. Med. Rehabil. 83 (2002) 903–906.
[54] S.R. Cummings, M.C. Nevitt, A hypothesis: the causes of hip fractures, J. Gerontol. 44 (1989) M107–M111.
[55] S. Majumder, A. Roychowdhury, S. Pal, Hip fracture and anthropometric variations: dominance among trochanteric soft tissue thickness, body height and body weight during sideways fall, Clin. Biomech. 28 (2013) 1034–1040.
[56] S. Majumder, A. Roychowdhury, S. Pal, Effects of trochanteric soft tissue thickness and hip impact velocity on hip fracture in sideways fall through 3D finite element simulations, J. Biomech. 41 (2008) 2834–2842.
[57] S.N. Robinovitch, T.A. McMahon, W.C. Hayes, Force attenuation in trochanteric soft tissues during impact from a fall, J. Orthop. Res. 13 (1995) 956–962.
[58] M.L. Bouxsein, P. Szulc, F. Munoz, E. Thrall, E. Sornay-Rendu, P.D. Delmas, Contribution of trochanteric soft tissues to fall force estimates, the factor of risk, and prediction of hip fracture risk, J. Bone Miner. Res. 22 (2007) 825–831.
[59] I.C. Levine, L.E. Minty, A.C. Laing, Factors that influence soft tissue thickness over the greater trochanter: application to understanding hip fractures, Clin. Anat. 28 (2) (2014).
[60] M.J. Bolland, A.T. Siu, B.H. Mason, A.M. Horne, R.W. Ames, A.B. Grey, et al., Evaluation of the FRAX and Garvan fracture risk calculators in older women, J. Bone Miner. Res. 26 (2011) 420–427.
[61] H.D. Nelson, M. Helfand, S.H. Woolf, J.D. Allan, Screening for postmenopausal osteoporosis: a review of the evidence for the US Preventive Services Task Force, Ann. Intern. Med. 137 (2002) 529–541.
[62] C. Boulay, C. Tardieu, J. Hecquet, C. Benaim, B. Mouilleseaux, C. Marty, et al., Sagittal alignment of spine and pelvis regulated by pelvic incidence: standard values and prediction of lordosis, Eur. Spine J. 15 (2006) 415–422.